

Lower sound speed and redshift induced by higher curvature effects

Sudan Hansraj,^{*} Megan Govender,[†] Lushen Moodly,[‡] and Ksh. Newton Singh[§]

Astrophysics and Cosmology Research Unit, School of Mathematics,

Statistics and Computer Science, University of KwaZulu-Natal,

Private Bag X54001, Durban 4000, South Africa

Department of Mathematics, Steve Biko Campus,

Durban University of Technology, Durban 4000, South Africa and

Department of Physics, National Defence Academy Khadakwasla, Pune-411023, India.

Faculty Council of Science, Jadavpur University, Kolkata-700032, India.

(Dated: April 21, 2020)

Abstract

We study the influence of higher curvature effects on stellar structure. A model of a superdense star with strange star equation of state is constructed within the framework of the Einstein–Gauss–Bonnet theory. Under these assumptions large classes of solutions are admitted by the field equations. We isolate a particular class with the ansatz of the Vaidya–Tikekar superdense star spatial gravitational potential. The model is found to satisfy elementary requirements for physical applicability. In particular, we obtain a pressure profile that is positive definite within a finite radius occurring at a hypersurface of vanishing pressure. Within the radius, the density profile, sound–speed behavior and energy conditions are all well behaved. The surface gravitational redshift function is consistent with the expectation for strange stars. Moreover, the adiabatic stability criterion of Chandrasekhar is satisfied as is the positivity of the difference between the sound speeds squared in the radial and transverse directions. A pleasing equation of state curve is evident for a particular choice of parameters. The mass profile and consequently the compactification index are all found to be reasonable. The parameter values chosen are consistent with observed star models. A significant effect of the higher curvature terms is to reduce the speed of sound and to drastically reduce the values of the surface gravitational redshift compared to the Einstein counterpart. These latter results have implications for observations in relativistic astrophysics which are often made against the background of the standard general theory of relativity.

PACS numbers: 04.20.Jb, 04.40.Nr, 04.70.Bw

* hansrajs@ukzn.ac.za

† megandhrehng@dut.ac.za

‡ lmoodly@gmail.com

§ ntnphy@gmail.com

I. INTRODUCTION

Alternate or extended theories of gravity have aroused considerable interest recently in view of difficulties with the general theory of relativity to explain anomalous behavior of gravitational phenomena such as the late time accelerated expansion of the universe (Riess et al. 1998; Perlmutter et al. 1999). One attempt at resolving the problem involves conjecturing the existence of exotic matter fields such as dark matter, dark energy, phantom fields and quintessence fields to name a few. To date there exists no experimental support for these ideas however a number of experiments are ongoing. In order to explain dark energy and dark matter de Rham [15] suggests that the graviton is not massless but actually carries a small mass. This itself has a number of ramifications for physics which has been dealt with elsewhere in the literature. An alternative approach is to re-examine the geometrical side of the field equations. Higher curvature effects may have a role to play. In particular, Einstein–Gauss–Bonnet (EGB) theory has proved promising in this regard, and therefore is extensively studied. Note that EGB belongs to a more general class of theories called the Lovelock polynomial Lagrangians which constitute the most general tensor theory generating at most second order equations of motion. If the Lagrangian is allowed to involve both tensor and scalar fields then the most general such theory is due to Horndeski (1974). A further strong motivation for EGB theory is that the Gauss–Bonnet Lagrangian appears in a natural way in the effective action of heterotic string theory in the low energy limit (Gross 1999). The causal structure of the singularities is different from general relativity for inhomogeneous distributions of dust and null dust (Ghosh, Jhingan & Deshkar 2014). The question we are probing is whether the addition of higher curvature gravitational effects play a significant role in the evolution of stars. Indeed most of our understanding of observations in relativistic astrophysics are made on the basis of Einstein’s theory of general relativity (GR). However, if GR is to be superseded by a higher curvature theory which preserves second order equations of motion and which reduces to GR in the solar system scale limit, then it is natural to ask what effect the higher curvature contributions have on stellar structure.

Historically black hole models in EGB theory have been thoroughly studied. Boulware & Deser (1985) generalized the higher dimensional solutions in Einstein theory due to Tangherlini (1963), and by Myers & Perry (1986) to include the contribution of the EGB theory with quadratic curvature terms. Wheeler (1986), Myers & Simons (1988) and Torii & Maeda

(2005) have also considered black hole solutions in EGB theory. Inhomogeneous collapse of dust, that is pressure-free fluid with non-interacting particles, was studied by Maeda (2006). However explicit exact solutions were obtained by Jhingan & Ghosh (2010). Dadhich, Molina & Khugaev (2010) proved that the constant density Schwarzschild interior solution is universal in the sense that it is valid in both higher dimensional Einstein theory as well as in EGB gravity. The matching of these exterior metrics to an interior for brane world stars to produce analytical models was investigated by Casadio and Ovalle (2014). The matching of isolated masses to a Schwarzschild exterior was analysed by Clifton et al. (2013).

The constant density configuration of Dadhich et al. (2010) was the first nontrivial compact star object in 5 dimensional EGB theory but unfortunately it suffers the drawback of having an infinite sound speed like its 4 dimensional counterpart thus making it non-physical. The static spherically symmetric star of Kang et al. (2012) needs to satisfy the junction conditions of EGB gravity so that matching is possible at the stellar hypersurface. The junction conditions for EGB were derived in Davis (2003) which are nontrivial and very different from general relativity. Note that the variable density model of Kang et al. (2012) requires a further integration to produce an exact solution. Variable density spherically symmetric exact solutions to the EGB field equations were first obtained by Hansraj et al. (2015), Chilambwe et al. (2015) and Maharaj et al. (2015) and shown to be consistent with the usual elementary expectations of astrophysical models. When one of the field equations is replaced by the equation of hydrodynamic equilibrium, namely the vanishing divergence of the energy momentum tensor, then it is prudent to invoke an equation of state relating the energy density and pressure. This appears to have been the approach of Kang et al. (2012) in their attempt to find an exact model. Interestingly the interior model presented in Kang et al. (2012) generates the well known vacuum metric (Boulware & Deser 1985) of EGB in the limit of vanishing pressure and density.

Local anisotropy in self-gravitating systems has been extensively studied within the framework of classical general relativity (Govender & Thirukkanesh 2015; Maurya, Ratanpal & Govender 2017; Maurya & Govender 2017; Maurya et al. 2019). The inclusion of pressure anisotropy in the study of compact objects such as pulsars, neutrons stars and quark stars in 4-D gravity has led to physically viable stellar models. Analyses of the physical attributes of these models such as density profiles, pressure profiles, compactness and surface redshift

agree with observed data within experimental error. The anisotropy parameter $\Delta = p_T - p_R$ can either be positive or negative at each interior point of the matter configuration. When $p_T > p_R$ the force due to local anisotropy is repulsive which may lead to more massive and stable configurations. A fruitful approach to generating physically realizable models of compact objects is to consider the idea of embedding a 4-dimensional spherically symmetric spacetime into a 5-dimensional Euclidean space. Karmarkar (1948) classified these spacetimes as embedding class-1. It is interesting to note that the Karmarkar condition in the presence of *pressure isotropy* leads to two exact models. The Kohler-Chao (1965) solution can be interpreted as of cosmological nature as there is no finite radius for which the radial pressure vanishes. The other exact model is the interior Schwarzschild solution which suffers from various pathologies such as superluminal sound speeds within the stellar core. Bowers & Liang (1974) demonstrated that the surface redshift can be arbitrarily large in the presence of pressure anisotropy. They were able to show that if the fractional anisotropy, $\frac{p_T - p_R}{p} > 0$, then the associated surface redshift is greater than its isotropic counterpart. The enhancement of the surface redshift is comparable to the magnitude of the anisotropy incorporated into the model. The role of anisotropy during dissipative collapse has yielded many interesting results (Maurya, Banerjee & Hansraj 2018). Herrera and co-workers have shown that the anisotropy affects the dynamical instability of the star undergoing collapse (Herrera, Le Denmat & Santos 1989; Chan, Herrera & Santos 1993; Herrera, Le Denmat & Santos 2012; Govender, Mewalal & Hansraj 2019). The stability factor Γ in both the Newtonian and post-Newtonian approximations deviate from the well-known result ($\Gamma > \frac{4}{3}$) first derived by Chandrasekhar (1964a). The sign of the anisotropic factor leads to a further deviation from the classical case. The presence of anisotropic stresses within the collapsing core can either advance or delay the formation of the horizon. From a thermodynamical point of view, it has been shown that pressure anisotropy leads to higher core temperatures. This effect is enhanced during the late stages of collapse when the differences in the anisotropic stresses are much larger (Govender et al. 2018).

Our intention in this paper is to solve the nonlinear EGB equations for a static spherically symmetric matter distribution with anisotropic stresses and with a strange star equation of state. In section II we briefly outline the basic equations in EGB gravity. The field equations in 5-dimensional EGB gravity are presented for a spherically symmetric metric, and they are then transformed to an equivalent form through a coordinate redefinition. In Section III

the generalized Vaidya–Tikekar (1982) superdense star ansatz is examined and a number of well known special cases are considered. In Section IV the physical features of the Finch–Skea model are investigated with the help of graphical plots and a comparison with the 5 dimensional Einstein counterpart is made. We make use of data associated with the X–ray pulsar LMC X–4 in order to determine the values of constants in the problem and from the plots we deduce that the model displays the necessary qualitative features expected of such astrophysical objects. Some concluding remarks are made in Section V.

II. EINSTEIN–GAUSS–BONNET GRAVITY

The Gauss–Bonnet action in five dimensions is written as

$$S = \int \sqrt{-g} \left[\frac{1}{2} (R - 2\Lambda + \alpha L_{GB}) \right] d^5x + S_{\text{matter}}, \quad (1)$$

where α is the dimensionfull Gauss–Bonnet coupling constant which may be identified with the string tension in string theory. Presently there are no experimental tests that constrain the value of the coupling constant and moreover it is not known whether α should necessarily be positive. In the work of Amendola *et al* (2007) it has been argued that the value of α may be as high as of the order of 10^{23} . These authors also considered solar system tests in the context of Einstein–Gauss–Bonnet theory. The strength of the action L_{GB} lies in the fact that despite the Lagrangian being quadratic in the Ricci tensor, Ricci scalar and the Riemann tensor, the equations of motion turn out to be second order quasilinear which is consistent with a theory of gravity. The Gauss–Bonnet term does not contribute to the dynamics of stellar evolution for $n \leq 4$ but is generally nonzero for $n > 4$. Specifically it has been shown that for the Gauss–Bonnet case only the dimensions 5 and 6 are necessary to consider. Because the 5-D case leads to some mathematical simplifications, it is not surprising that practically all investigations in the literature have avoided the 6-D case.

The EGB field equations may be written as

$$G_{ab} + \alpha H_{ab} = T_{ab}, \quad (2)$$

where we have adopted the metric signature $(-+++)$ and where G_{ab} is the usual Einstein tensor. The Lanczos tensor is given by

$$H_{ab} = 2 \left(R R_{ab} - 2 R_{ac} R_b^c - 2 R^{cd} R_{acbd} + R_a^{cde} R_{bcde} \right) - \frac{1}{2} g_{ab} L_{GB}, \quad (3)$$

where the Lovelock term has the form

$$L_{GB} = R^2 + R_{abcd}R^{abcd} - 4R_{cd}R^{cd}. \quad (4)$$

Now varying the action against the metric generate the Einstein–Gauss–Bonnet equations of motion which we display below.

III. FIELD EQUATIONS

The generic 5-dimensional line element for static spherically symmetric spacetimes is taken as

$$ds^2 = -e^{2\nu}dt^2 + e^{2\lambda}dr^2 + r^2(d\theta^2 + \sin^2\theta d\phi^2 + \sin^2\theta \sin^2\phi d\psi^2), \quad (5)$$

where $\nu(r)$ and $\lambda(r)$ are the gravitational potentials. We utilise a comoving fluid velocity of the form $u^a = e^{-\nu}\delta_0^a$ and the matter field is that of a perfect fluid with energy momentum tensor $T_{ab} = (\rho + p)u_a u_b + pg_{ab}$. Accordingly the EGB field equations (2) reduce to

$$\rho = \frac{3}{e^{4\lambda}r^3} (4\alpha\lambda' + re^{2\lambda} - re^{4\lambda} - r^2e^{2\lambda}\lambda' - 4\alpha e^{2\lambda}\lambda'), \quad (6)$$

$$p_R = \frac{3}{e^{4\lambda}r^3} (-re^{4\lambda} + (r^2\nu' + r + 4\alpha\nu')e^{2\lambda} - 3\alpha\nu'), \quad (7)$$

$$\begin{aligned} p_T = & \frac{1}{e^{4\lambda}r^2} \left(-e^{4\lambda} - 4\alpha\nu'' + 12\alpha\nu'\lambda' - 4\alpha(\nu')^2 \right) \\ & + \frac{1}{e^{2\lambda}r^2} \left(1 - r^2\nu'\lambda' + 2r\nu' - 2r\lambda' + r^2(\nu')^2 \right) \\ & + \frac{1}{e^{2\lambda}r^2} \left(r^2\nu'' - 4\alpha\nu'\lambda' + 4\alpha(\nu')^2 + 4\alpha\nu'' \right). \end{aligned} \quad (8)$$

where the subscripts R and T refer to the radial and transverse components respectively. The system (6)–(8) comprises three field equations in five unknowns and is trivially solved by choosing any arbitrary metric. This approach is however unlikely to yield exact models that conform to the elementary tests for physical viability. Accordingly inserting some constraints of physical importance will likely give solutions that may be used to model compact stars. In this work, we prescribe a strange star equation of state and this immediately increases the mathematical complexity. However, there remains one more prescription to make to close the system. We shall employ a metric ansatz of a superdense star in order to determine a unique solution. Observe that the vacuum metric describing the gravitational field exterior

to the 5-dimensional static perfect fluid may be described by the Boulware–Deser (1985) spacetime as

$$ds^2 = -F(r)dt^2 + \frac{dr^2}{F(r)} + r^2 (d\theta^2 + \sin^2 \theta d\phi + \sin^2 \theta \sin^2 \phi d\psi), \quad (9)$$

where

$$F(r) = 1 + \frac{r^2}{4\alpha} \left(1 - \sqrt{1 + \frac{8M\alpha}{r^4}} \right).$$

In the above M is associated with the gravitational mass of the hypersphere. The exterior solution is unique up to branch cuts, however, there appears to be no equivalent of the Birkhoff theorem of the 4-dimensional Einstein gravity case. Bogdanos et al. (2009) have investigated the 6-dimensional case in EGB and demonstrated that Birkhoff’s theorem holds for particular assumptions. At this point we also note that the Buchdahl (1959) compactness limit for a perfect fluid sphere $\frac{M}{R} = \frac{4}{9}$ was recently improved to the case of 5 dimensional EGB (Wright 2016) but the results depend on sign of the coupling constant α .

To enhance our chances of locating exact solutions, we make the following change of variables $e^{2\nu} = y^2(x)$, $e^{-2\lambda} = Z(x)$ and $x = Cr^2$ (C being an arbitrary constant). This set of transformations has proved particularly useful in the case of isotropic fluids since the isotropy equation may be written as linear differential equations in either variable y or Z in Einstein gravity. In EGB, the same equation is linear in y but nonlinear in Z . For applications of this approach to charged anisotropic relativistic matter see the recent works of Mafa Takisa & Maharaj (2013) and Maharaj, Sunzu & Ray (2014) in four dimensional Einstein theory. The field equations (6)–(8) may now be expressed as

$$-3\dot{Z} - \frac{3(Z-1)(1-\beta\dot{Z})}{x} = \frac{\rho}{C}, \quad (10)$$

$$\frac{3(Z-1)}{x} + \frac{6Z\dot{y}}{y} - \frac{6\beta(Z-1)Z\dot{y}}{xy} = \frac{p_R}{C}, \quad (11)$$

$$\begin{aligned} & 4Z [\beta(1-Z) + x] \frac{\ddot{y}}{y} \\ & + \left[\frac{2\beta Z(1-Z)}{x} + 2(x+\beta)\dot{Z} + 6Z(1-\beta\dot{Z}) \right] \frac{\dot{y}}{y} \\ & + \left[\frac{Z-1}{x} + 2\dot{Z} \right] = \frac{p_T}{C}, \end{aligned} \quad (12)$$

where we have introduced the constant $\beta = 4\alpha C$ containing the EGB coupling constant.

We now utilise a physically important equation of state relating the density and pressure. The prescription $p_R = \gamma\rho - \xi$ is understood to be valid for strange star material or quark stars which have a higher density and larger rotation than neutron stars. The special case $\gamma = \frac{1}{3}$ corresponds to the well studied MIT Bag model where quarks are considered as free particles and their thermodynamic properties are generated by treating them as an Fermi (ideal) gas. With this equation of state (10) and (11) together yield

$$\frac{\dot{y}}{y} = \left[6Z - \frac{6\beta(Z-1)Z}{x} \right]^{-1} \left[3\gamma\dot{Z} + \frac{3(Z-1)(\gamma-1-\beta\gamma Z)}{x} - \xi \right] \quad (13)$$

where γ and $\beta \geq 0$ are constants. Equation (13) integrates as

$$y = C_1 \exp \left(\int \frac{3\gamma x \dot{Z} + 3(Z-1)(\gamma-1-\beta\gamma Z) - \xi x}{6xZ - 6\beta(Z-1)Z} dx \right) \quad (14)$$

where C_1 is an integration constant. It now remains to detect forms for Z that will permit the complete integration of (14).

IV. VAIDYA-TIKEKAR SUPERDENSE STAR ANSATZ

Equation (14) admits a large number of potentials Z for which an exact solution exists. Therefore, it is prudent to make a selection from well studied models which are known to be physically reliable. Expressed in terms of our coordinates the generalised Vaidya–Tikekar potential prescription, known to generate super-dense stellar models (Vaidya & Tikekar 1982), is given by

$$Z = \frac{1 + ax}{1 + bx} \quad (15)$$

where a and b are arbitrary real numbers related to the spheroidal parameter. Note that specifying the spatial metric potential is tantamount to determining the law of variation of the density profile. The special case $b = 0$ corresponds to the constant density Schwarzschild interior solution while the case $a = 0$ is the Finch–Skea (1989) ansatz first proposed by Duorah & Ray (1987). An exact solution for spheroidally distributed matter was examined in the case $a = -1$ and $b = 2$ by Vaidya and Tikekar (Vaidya & Tikekar 1982) and shown to admit models with surface densities $2 \times 10^{14} \text{ g/cm}^3$ with masses of about 4 times the solar mass. The choice $b = 1$ was studied by Buchdahl (1959,1984) and recently Molina *et al* used this ansatz to find models of stars in pure Gauss–Bonnet gravity (Molina, Dadhich

& Khugaev 2017). The general integral of (14) has the form

$$\begin{aligned}
y = \exp \left(\frac{1}{6} (a^2 ((-3a^2\beta^2\gamma + a\beta(b(3(\beta+1)\gamma - \beta\xi - 3) + 3\gamma) \right. \\
\left. + b(b\beta(\beta\xi - 3\gamma + 3) - 3(\beta - 1)\gamma)) \log(-a\beta + b(\beta + x) + 1)) \right. \\
\left. - b(\log(ax + 1) (a^2(6\gamma - 3) - a(3b(\gamma - 1) + \xi) + b\xi)) - ab^2\xi x) / (ab(a\beta - 1)) \right) \quad (16)
\end{aligned}$$

for the potential (15).

A. Schwarzschild incompressible star

The choice $Z = 1 + x$ is known to generate a constant density fluid sphere by equation (10). For this case (16) reduces to

$$y = \exp \left(\frac{3a\beta\gamma(ax + 1) + (-6a\gamma + 3a + \xi) \log(ax + 1)}{6a(a\beta - 1)} \right) \quad (17)$$

which is not the same temporal potential as for the isotropic Schwarzschild sphere. In respect of the proposed strange star equation of state we are considering the energy density, radial and tangential pressures evaluate to

$$\rho = 3a(-\beta a + 2) \quad (18)$$

$$p_R = \frac{\xi(1 - a\beta) - 3a\gamma(a\beta - 1)(a\beta x + \beta - 2)}{a\beta - 1} \quad (19)$$

$$\begin{aligned}
p_T = & \frac{-9a}{(a\beta - 1)^2(ax + 1)} \\
& - \frac{3(\beta(x(a(x(ax + 5) - 2) + 4) - 1) - x(2ax + 3))(3a(\gamma(a\beta x + \beta - 2) + 1) + \xi)}{x(a\beta - 1)^3(ax + 1)^2} \\
& + \frac{x(1 - a\beta)(6a(1 - a\beta)(a(3 - 6\gamma) + \xi) + (3a(\gamma(a\beta x + \beta - 2) + 1) + \xi)^2)}{(a\beta - 1)^2(ax + 1)} \quad (20)
\end{aligned}$$

where we have set $C = 1$. We neglect conducting a more comprehensive analysis of this particular solution in light of the fact that the sound speed being infinite is not physically viable. We concentrate on a solution that has potential to model realistic stars below.

B. Finch Skea spatial potential

The Finch–Skea potential $Z = \frac{1}{1+x} = \frac{1}{1+Cr^2}$ was used to model four dimensional static stars with behaviors consistent with the astrophysical theory of Walecka (1975). It is also well known that for regular stars, that is models that are singularity-free, it is necessary that the spatial potential has the form $1 + O(r^2)$. This proves to be useful in this higher curvature analysis as well and it will be observed that all physical quantities are free of the defect of being singular somewhere within the distribution. For the Finch–Skea prescription the potential (16) assumes the simplified form

$$y = A(\beta + v)^{a_1} e^{-\frac{1}{12}(a_2 + \xi x)(\beta + v)} \quad (21)$$

where we make the substitutions $a_1 = \frac{1}{6}(3\beta\gamma - \beta(\beta\xi - 3\gamma + 3) - 3\gamma)$, $a_2 = 6\xi\gamma - 3\xi\beta + \xi - 6$, $w_1 = 1 + x$, $w_2 = 1 + x + \beta$ and $w_3 = 1 + 2x + \beta$ to shorten the lengthy expressions to follow. The associated dynamical quantities have the form

$$\frac{\rho}{C} = \frac{3(\beta + x(w_1 + 2) + 2)}{w_1^3} \quad (22)$$

$$\frac{p_R}{C} = \frac{12a_1 - a_2w_2 - \xi w_2w_3 - 6w_1}{2w_1^2} \quad (23)$$

$$\begin{aligned} \frac{p_T}{C} = & \left[-6\xi (3(\beta + 1)^2 + 8x^3 + (6\beta + 20)x^2 + 15(\beta + 1)x) - 36w_1(x + 3) + 2\xi xw_1w_2w_3 \right. \\ & \left. + \frac{144a_1^2xw_1}{w_2}\xi^2 + xw_1w_2w_3^2 + a_2(a_2xw_1w_2 - 6(3\beta + 2x^2 + 5x + 3)) \right] / 36w_1^3 \end{aligned} \quad (24)$$

while the measure of the pressure anisotropy $\Delta = p_T - p_R$ is given by the expression

$$\begin{aligned} \frac{\Delta}{C} = & [72w_1 - 6\xi (-3\beta^2 - 3\beta x + x(2x + 5) + 3) + \xi^2w_1w_2w_3^2 \\ & + \frac{144a_1^2w_1}{w_2} - 24a_1(a_2w_1 + \xi w_1w_3 + 9) \\ & + a_2(a_2w_1w_2 + 2\xi w_1w_2w_3 + 6(3\beta + x + 1))] / 36w_1^2 \end{aligned} \quad (25)$$

Observe that a hypersurface of vanishing pressure exists when $p_R = 0$ demarcating the boundary of the 5 dimensional hypersphere at

$$x = \frac{1 - 2a_1\beta - 2a_1 - 2a_2}{2a_1 - 1} \quad (26)$$

in terms of the constants associated with the strange star equation of state and Gauss–Bonnet coupling constant. The ratio of the pressure to the energy density $\frac{p}{\rho}$ is understood to give an indication of the equation of state of the model. In this case we obtain

$$\left(\frac{p}{\rho}\right)_R = \frac{w_1 (12a_1 - a_2 w_2 - \xi w_2 w_3 - 6w_1)}{6(\beta + x(x + 3) + 2)} \quad (27)$$

$$\begin{aligned} \left(\frac{p}{\rho}\right)_T = & [-36w_1(x + 3) - 6\xi (3(\beta + 1)^2 + 8x^3 + (6\beta + 20)x^2 + 15(\beta + 1)x) \\ & + \frac{144a_1^2 x w_1}{\beta + x + 1} + \xi^2 + x w_1 w_2 w_3^2 - 24a_1 (a_2 x w_1 + \xi x w_1 w_3 - 9) \\ & + a_2 (a_2 x w_1 w_2 - 6 (3\beta + 2x^2 + 5x + 3) + 2\xi x w_1 w_2 w_3)] / 108(\beta + x(x + 3) + 2) \end{aligned} \quad (28)$$

for the radial and transverse components. The causal behavior of stars is studied by examining the square of the sound speed given by the formula $v^2 = \frac{dp}{d\rho}$. This evaluates to

$$v_R^2 = -\frac{w_1 (a_2(2\beta + x + 1) - 24a_1 + \xi (2\beta^2 + \beta + 3\beta x - x - 1) + 6w_1)}{6 (3\beta + x^2 + 4x + 3)} \quad (29)$$

$$\begin{aligned} v_T^2 = & -\{ 36w_1(x + 5) + 6\xi (9\beta^2 + 3\beta + 6\beta x(x + 3) - 2w_1(2x + 3)) \\ & + \xi^2 w_1 w_3 ((\beta + 1)^2 + 4x^3 + 2(\beta + 5)x^2 - (\beta - 7)(\beta + 1)x) \\ & - \frac{144a_1^2 w_1 (2x^2 + \beta(x - 1) + x - 1)}{w_2^2} \\ & + 24a_1 (a_2 (x^2 - 1) + \xi w_1 (\beta(x - 1) - 3x - 1) - 27) \\ & + a_2 [2\xi w_1 ((\beta + 1)^2 + 2x^3 + 6x^2 - (\beta - 5)(\beta + 1)x) + 6(9\beta + 2x(x + 3) + 4)] \\ & + a_2^2 (\beta + x(-\beta x + x + 2) + 1) \} / 108 (3\beta + x^2 + 4x + 3) \end{aligned} \quad (30)$$

and the expectation is that both these quantities should be constrained in the interval $(0; 1)$ to guarantee that the sound speed remains subluminal. The possibility of superluminal behavior in ultrabaric matter in special relativity was discussed by Caporaso and Bescher (1979) and ruled out. The difference between the squares of the radial and transverse sound

speeds given by

$$\begin{aligned}
v_R^2 - v_T^2 = & \{324w_1^2 [a_2(2\beta + x + 1) - 24a_1 + \xi (2\beta^2 + \beta + 3\beta x - x - 1) + 6w_1]^2 \\
& - [6\xi (9\beta^2 + 3\beta + 6\beta x(x + 3) - 2w_1(2x + 3)) + 36w_1(x + 5) \\
& + \xi^2 w_1 w_3 ((\beta + 1)^2 + 4x^3 + 2(\beta + 5)x^2 - (\beta - 7)(\beta + 1)x) \\
& - \frac{144a_1^2 w_1 (2x^2 + \beta(x - 1) + x - 1)}{w_2^2} \\
& + 24a_1 (a_2 (x^2 - 1) + \xi w_1 (\beta(x - 1) - 3x - 1) - 27) \\
& + a_2 (2\xi w_1 ((\beta + 1)^2 + 2x^3 + 6x^2 - (\beta - 5)(\beta + 1)x) + 6(9\beta + 2x(x + 3) + 4)) \\
& a_2^2 (\beta + x(-\beta x + x + 2) + 1)]^2\} / 11664 (3\beta + x^2 + 4x + 3)^2
\end{aligned} \tag{31}$$

provides an indication of the stability of the model. Graphical plots will be used to analyse these features. The active gravitational mass is computed via the formula $\frac{1}{3} \int \rho r^{d-2} dr$ where d is the spacetime dimension. In the five dimensional case we obtain

$$M(r) = \frac{k}{3} + \frac{1}{2C^2} \left(x - \frac{\beta + 2(\beta - 1)x - 2}{2w_1^2} \right) \tag{32}$$

and correspondingly the compactification parameter

$$\frac{M(r)}{r} = \left[\frac{k}{3} + \frac{1}{2C^2} \left(x - \frac{\beta + 2(\beta - 1)x - 2}{2w_1^2} \right) \right] \times \sqrt{\frac{c}{x}} \tag{33}$$

will be useful in determining whether the Buchdahl limit for the mass-radius ratio applicable to Einstein stars is still valid when higher curvature effects are included.

Another indicator of stability devised by Chandrasekhar (1964a, 1964b) is the adiabatic

stability parameter $\Gamma = \left(\frac{\rho+p}{p} \right) \frac{dp}{d\rho}$ which assume the forms

$$\Gamma_R = \frac{(a_2(2\beta + x + 1) - 24a_1 + \xi(2\beta^2 + \beta + 3\beta x - x - 1) + 6w_1)}{6(3\beta + x^2 + 4x + 3)(a_2w_2 - 12a_1 + \xi w_2w_3 + 6w_1)} \times \frac{(w_2(a_2w_1 + \xi w_1w_3 - 6) - 12a_1w_1)}{6(3\beta + x^2 + 4x + 3)(a_2w_2 - 12a_1 + \xi w_2w_3 + 6w_1)} \quad (34)$$

$$\begin{aligned} \Gamma_T = & -\{36(3\beta + 2x^2 + 5x + 3) - 6\xi(3(\beta + 1)^2 + 8x^3 + (6\beta + 20)x^2 + 15(\beta + 1)x) \\ & - 24a_1(a_2xw_1 + \xi xw_1w_3 - 9) + \frac{144a_1^2xw_1}{\beta + x + 1} + \xi^2 + xw_1w_2w_3^2 \\ & + a_2(a_2xw_1w_2 - 6(3\beta + 2x^2 + 5x + 3) + 2\xi xw_1w_2w_3)\} \\ & \times \{6\xi(9\beta^2 + 3\beta + 6\beta x(x + 3) - 2w_1(2x + 3)) + 36w_1(x + 5) \\ & + \xi^2w_1w_3((\beta + 1)^2 + 4x^3 + 2(\beta + 5)x^2 - (\beta - 7)(\beta + 1)x) \\ & + 24a_1(a_2(x^2 - 1) + \xi w_1(\beta(x - 1) - 3x - 1) - 27) \\ & - \frac{144a_1^2w_1(2x^2 + \beta(x - 1) + x - 1)}{w_2^2} \\ & + a_2[2\xi w_1((\beta + 1)^2 + 2x^3 + 6x^2 - (\beta - 5)(\beta + 1)x) + 6(9\beta + 2x(x + 3) + 4)] \\ & + a_2^2(\beta + x(-\beta x + x + 2) + 1)\} / \{108(3\beta + x^2 + 4x + 3) \\ & \times [-6\xi(3(\beta + 1)^2 + 8x^3 + (6\beta + 20)x^2 + 15(\beta + 1)x) - 36w_1(x + 3) \\ & + \frac{144a_1^2xw_1}{\beta + x + 1} + \xi^2 + xw_1w_2w_3^2 - 24a_1(a_2xw_1 + \xi xw_1w_3 - 9) \\ & + a_2(2\xi xw_1w_2w_3 - 6(3\beta + 2x^2 + 5x + 3)) + a_2^2xw_1w_2]\} \end{aligned} \quad (35)$$

for the anisotropic model under consideration. Adiabatic stability occurs provided that Γ exceeds the critical value $\frac{4}{3}$. For a recent study of this property in the context of neutron stars see the work of Koliogiannis & Moustakidis (2019). The gravitational surface redshift z obtained from the formula $z = e^{-\nu} - 1$ is given by

$$z = \frac{1}{A} w_2^{-a_1} e^{\frac{1}{12}w_2(a_2+\xi x)} - 1 \quad (36)$$

for our model. The energy conditions for anisotropic matter may be investigated with the help of the expressions $\rho - p$ (weak energy condition, $\rho + p$ (strong energy condition and

$\rho + 3p$ the dominant energy condition. For the radial and transverse directions we obtain

$$\frac{(\rho - p)_R}{C} = [w_1 (a_2 w_2 - 12a_1 + \xi w_2 w_3 + 6w_1) + 6(\beta + x(x + 3) + 2)] / 2w_1^3 \quad (37)$$

$$\begin{aligned} \frac{(\rho - p)_T}{C} = & \{36 (3\beta + 4x^2 + 13x + 9) + 6\xi [3(\beta + 1)^2 + 8x^3 + (6\beta + 20)x^2 + 15(\beta + 1)x] \\ & - \xi^2 x w_1 w_2 w_3^2 - \frac{144a_1^2 x w_1}{\beta + x + 1} + 24a_1 (a_2 x w_1 + \xi x w_1 w_3 - 9) - a_2^2 x w_1 w_2 \\ & + a_2 [18(\beta + 1) - 2\xi x w_1 w_2 w_3 + 6x(2x + 5)]\} / 36w_1^3 \end{aligned} \quad (38)$$

$$\frac{(\rho + p)_R}{C} = \frac{12a_1 w_1 - w_2 (a_2 w_1 + \xi w_1 w_3 - 6)}{2w_1^3} \quad (39)$$

$$\begin{aligned} \frac{(\rho + p)_T}{C} = & \{36 (3\beta + 2x^2 + 5x + 3) - 6\xi [3(\beta + 1)^2 + 8x^3 + (6\beta + 20)x^2 + 15(\beta + 1)x] \\ & + \frac{144a_1^2 x w_1}{\beta + x + 1} + \xi^2 + x w_1 w_2 w_3^2 - 24a_1 (a_2 x w_1 + \xi x w_1 w_3 - 9) \\ & + a_2 [a_2 x w_1 w_2 - 6 (3\beta + 2x^2 + 5x + 3) + 2\xi x w_1 w_2 w_3]\} / 36w_1^3 \end{aligned} \quad (40)$$

$$\begin{aligned} \frac{\rho + 3p}{C} = & \{3\xi [9(\beta + 1)^2 + 22x^3 + (21\beta + 55)x^2 + 3(\beta + 1)(\beta + 14)x] + 18 [3(\beta + 5) \\ & + x(8x + 23)] - \xi^2 x w_1 w_2 w_3^2 - \frac{144a_1^2 x w_1}{\beta + x + 1} + 12a_1 (2a_2 x w_1 + 2\xi x w_1 w_3 - 9(x + 3)) \\ & + a_2 [-a_2 w_1 x w_2 + 21x^2 - 2\xi w_1 x w_2 w_3 + 9\beta(x + 3) + 48x + 27]\} / 18w_1^3 \end{aligned} \quad (41)$$

V. PHYSICAL ANALYSIS

In this section we discuss the physical plausibility of our compact star model. In order to generate the plots we have utilized mass and radius data associated with the pulsar LMC X-4 which qualifies as a superdense star to determine integration constants while other constants were assigned special values through fine-tuning. Specifically we have utilized values of the Gauss-Bonnet coupling α of the order of 10^3 as these values generate physically pleasing plots. Note that in this investigation we are using geometric units in which the gravitational constant G and the speed of light c are both set to unity. For this reason we cannot make quantitative determinations on the value of α . The study does offer us an avenue to make qualitative conclusions from the illustrative values of α and to contrast with the Einstein scenario when $\alpha = 0$. In Fig. 1 the density is shown to be a smooth singularity-free monotonically decreasing function of the radial coordinate. We observe that the density decreases with an increase in magnitude of the coupling constant. Figure 2. shows that the radial and tangential pressures decrease monotonically outwards towards the stellar surface. This is expected as the density in the central regions of the star is much higher than the surface density. It is interesting to note that the radial pressure is greater than the tangential pressure for large values of the coupling constant. This means that the force due to the pressure anisotropy is attractive in this regime. As the coupling constant decreases the tangential pressure dominates the radial pressure leading to a repulsive contribution from the anisotropy. Most importantly a hypersurface of vanishing radial pressure is clearly visible for a radial value of approximately 8.3 km. The behavior of all physical quantities should be studied within this radius. The central pressure is well behaved displaying no singularities for any value of the coupling constant α . Observations of the adiabatic stability index Γ in Figure 3. shows that the fluid is more stable for increasing α . This implies that higher order corrections tend to make the compact object more stable against perturbations. The critical lower bound of $\frac{4}{3}$ established by Chandrasekhar for Einstein gravity is always exceeded for both tangential and transverse directions. Causality is obeyed throughout the fluid configuration as exhibited in Figure 4. Both the radial and tangential speed of sound lie within the bounds $(0, 1)$. The equation of state parameter is an important indicator of the relationship between the pressure and density at each interior point of the star. From Figure 5. we observe that the ratio of the pressure to density increases with an increase in

the coupling constant. This implies that stronger contributions from higher corrections lead to more compact objects. In Figure 6. we observe that the anisotropy changes sign which implies that force associated with anisotropy can be repulsive ($p_T > p - R$) or attractive ($p_T < p_R$). Lower order contributions (smaller values of α) lead to repulsive effects due to anisotropy. All the energy conditions being positive as displayed in Figure 7. are satisfied. The metric potentials are continuous and well-behaved throughout the star as evidenced in Figure 8. The surface redshift is illustrated in Figure 9. We observe that the surface redshift is higher for smaller values of α which supports our observation of the density increasing with smaller values of the coupling constant (Figure 1). The forces required for equilibrium are illustrated in Figure 11. In order to achieve equilibrium we require that $F_g + F_h + F_a = 0$ where F_g , F_h and F_a are the gravitational, hydrostatic and anisotropic forces respectively. Figure 12 displays the variation of the mass with respect to the radius. Clearly within the stellar radius 8.3 km there appears to be little difference in the mass profile for various α values. If the gravitational field admitted a higher radial value then the plot displays that a maximum mass is achieved and some discrimination in values occur near this maximum.

The frames in Figure 13 to Figure 15 display the various physical quantities of our compact model in the 5D classical Einstein limit (ie., $\alpha = 0$). Radial quantities are in red while transverse items are in black. We observe that the respective quantities such as density, pressures, redshift and anisotropy are all substantially higher than their EGB counterparts hence the need for separate plots. Xian-Feng & Huan-Yu (2014) established that through relativistic mean field theory that the surface gravitational redshift of the star PSR J0348+0432 is in the region of about 0.3473 to 0.4064 which was higher than the canonical mass neutron star with a redshift of 0.226. Our 5D stellar model (Figure 14) displays a redshift in the range 0.15 to 0.22 within the distribution. This is therefore comparable with a neutron star. Note that when higher curvature terms are present as depicted in Figure 9, the surface redshift drops dramatically to the range of order 0.0025 to 0.0050. Figure 14 also demonstrates that the measure of anisotropy, the energy conditions and the speed of sound are all within the expected levels. The stability measures shown in Figure 15 confirm that the 5D Einstein model is stable with a well behaved mass profile. These stability features are not disturbed by the introduction of higher curvature effects due to the Gauss-Bonnet action. In Table 1 we exhibit a few stellar models which fall in the range of the mass and radius comparable to LMC X-4. This shows that our qualitative results are consistent with a large number of

known stars.

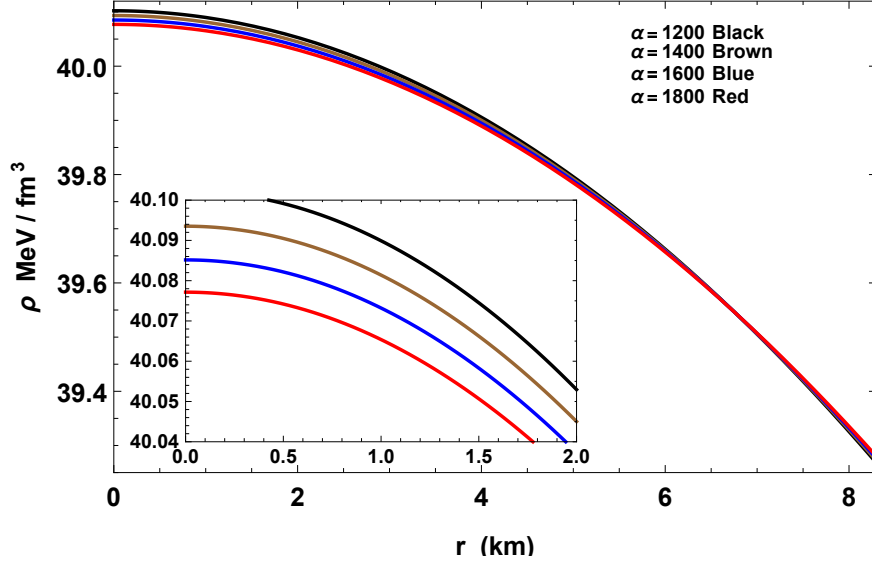


FIG. 1. Variation of density ρ with radial coordinate for LMC X-4 with $M = 1.04M_{\odot}$, $R = 8.3\text{km}$ and $\gamma = 1/3$ in EGB.

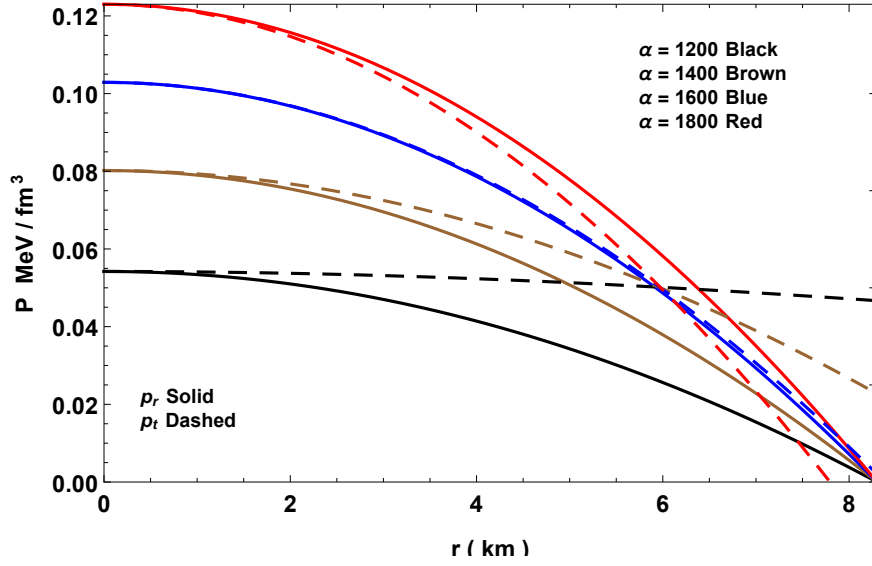


FIG. 2. Variation of pressures p with radial coordinate for LMC X-4 with $M = 1.04M_{\odot}$, $R = 8.3\text{km}$ and $\gamma = 1/3$ in EGB.

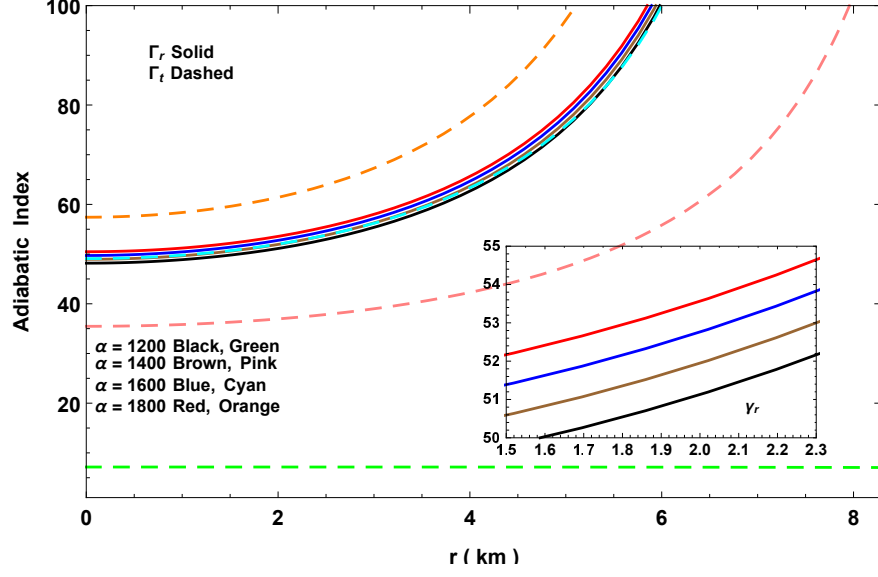


FIG. 3. Variation of adiabatic index Γ with radial coordinate for LMC X-4 with $M = 1.04M_{\odot}$, $R = 8.3km$ and $\gamma = 1/3$ in EGB.

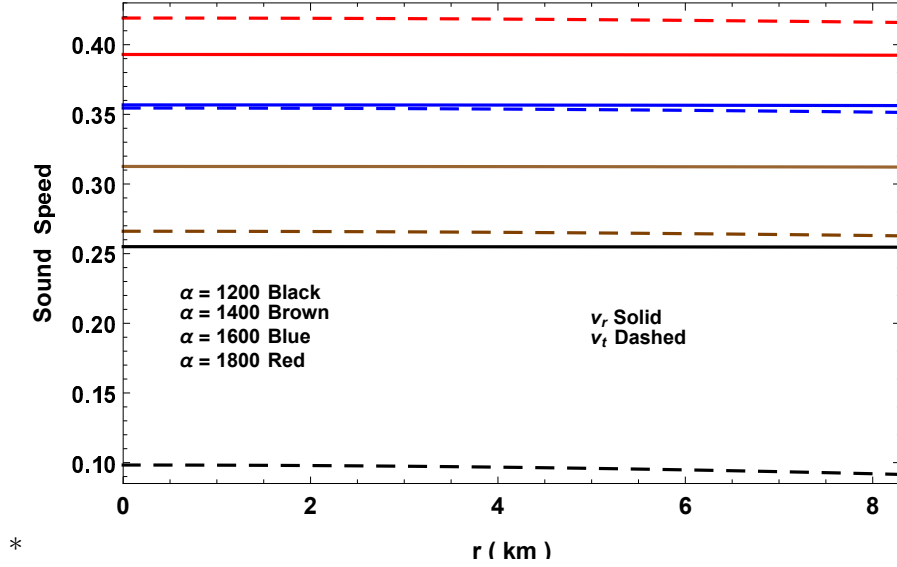


FIG. 4. Variation of sound speed with radial coordinate for LMC X-4 with $M = 1.04M_{\odot}$, $R = 8.3km$ and $\gamma = 1/3$ in EGB.

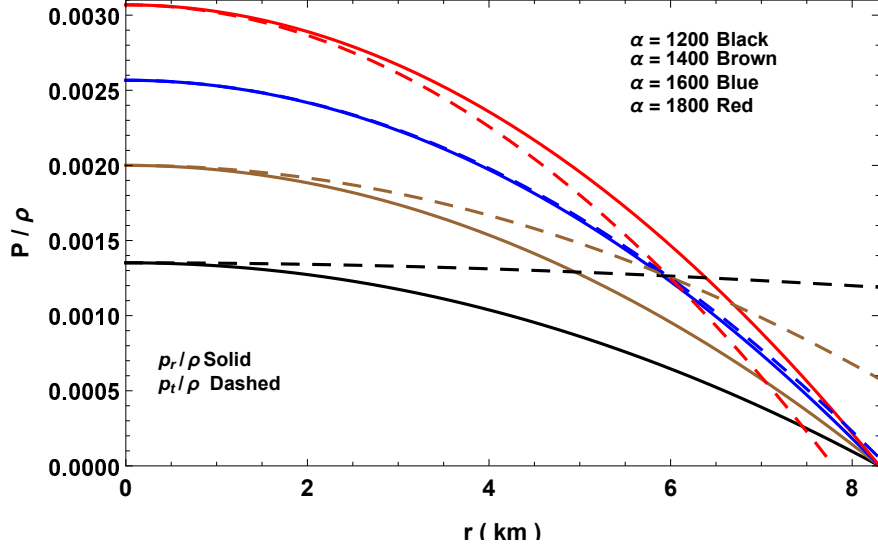


FIG. 5. Variation of equation of state parameters with radial coordinate for LMC X-4 with $M = 1.04M_{\odot}$, $R = 8.3km$ and $\gamma = 1/3$ in EGB.

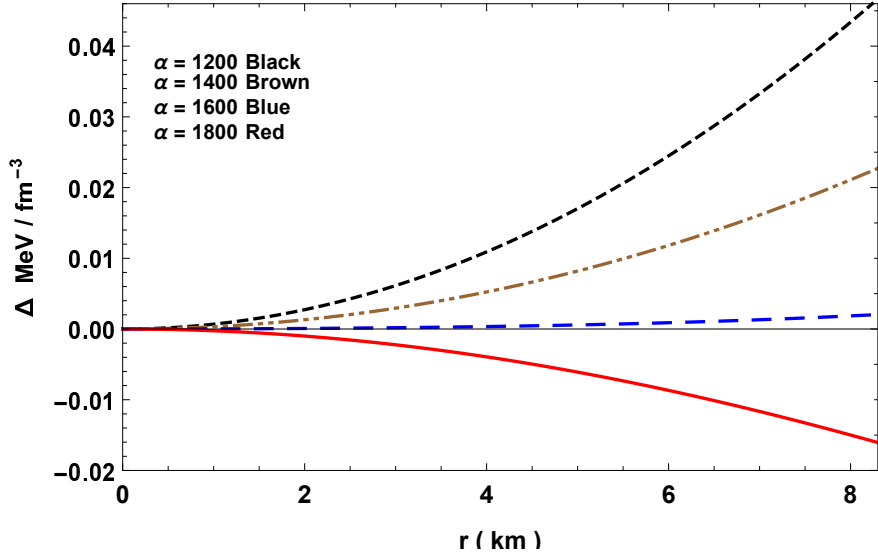


FIG. 6. Variation of anisotropy with radial coordinate for LMC X-4 with $M = 1.04M_{\odot}$, $R = 8.3km$ and $\gamma = 1/3$ in EGB.

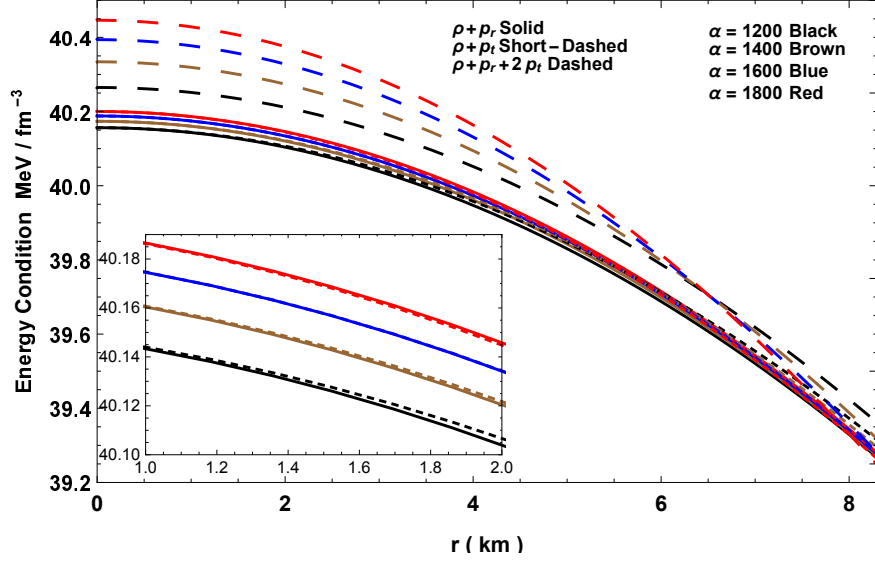


FIG. 7. Variation of energy conditions with radial coordinate for LMC X-4 with $M = 1.04M_{\odot}$, $R = 8.3km$ and $\gamma = 1/3$ in EGB.

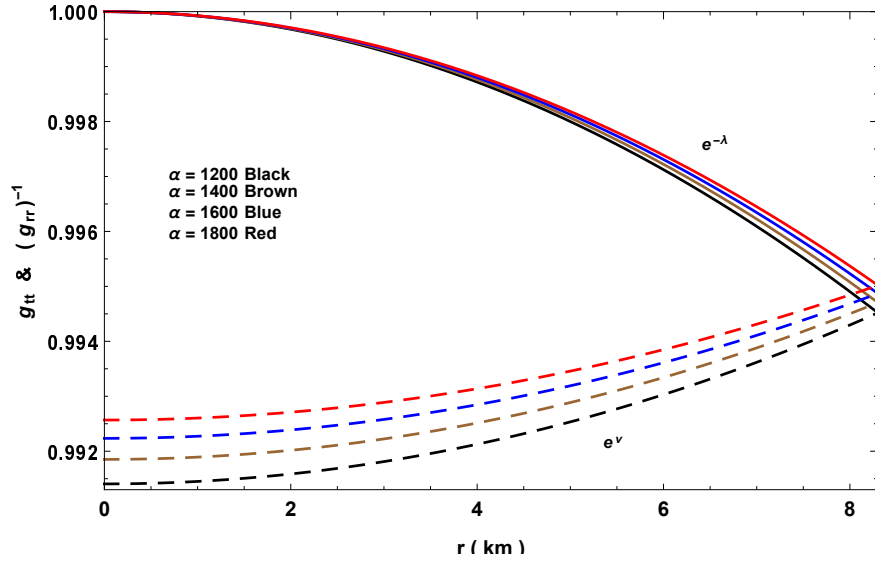


FIG. 8. Variation of metric potentials with radial coordinate for LMC X-4 with $M = 1.04M_{\odot}$, $R = 8.3km$ and $\gamma = 1/3$ in EGB.

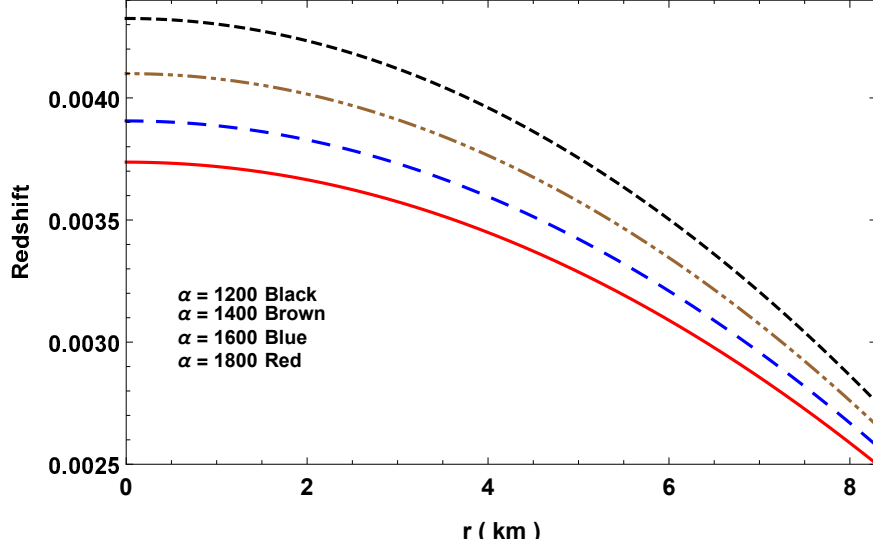


FIG. 9. Variation of red-shift with radial coordinate for LMC X-4 with $M = 1.04M_{\odot}$, $R = 8.3km$ and $\gamma = 1/3$ in EGB.

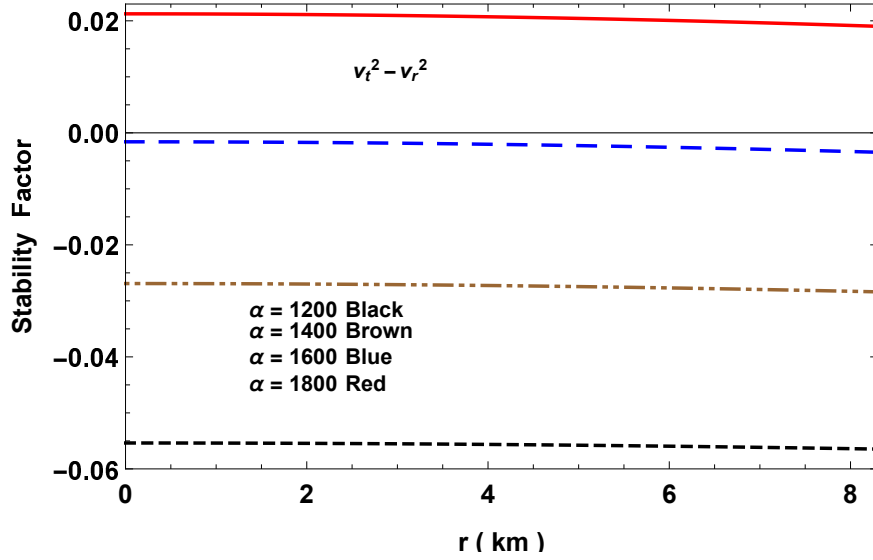


FIG. 10. Variation of stability factor with radial coordinate for LMC X-4 with $M = 1.04M_{\odot}$, $R = 8.3km$ and $\gamma = 1/3$ in EGB.

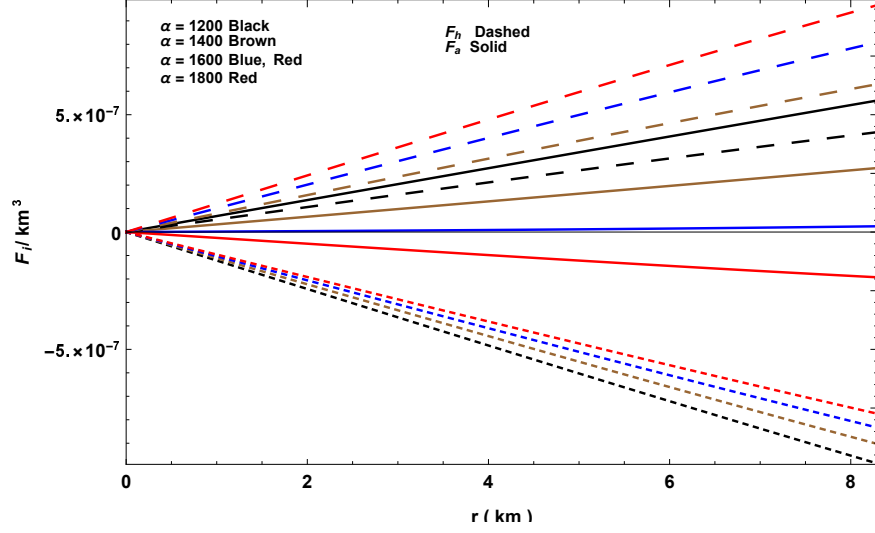


FIG. 11. Variation of forces in TOV-equation with radial coordinate for LMC X-4 with $M = 1.04M_{\odot}$, $R = 8.3km$ and $\gamma = 1/3$ in EGB.

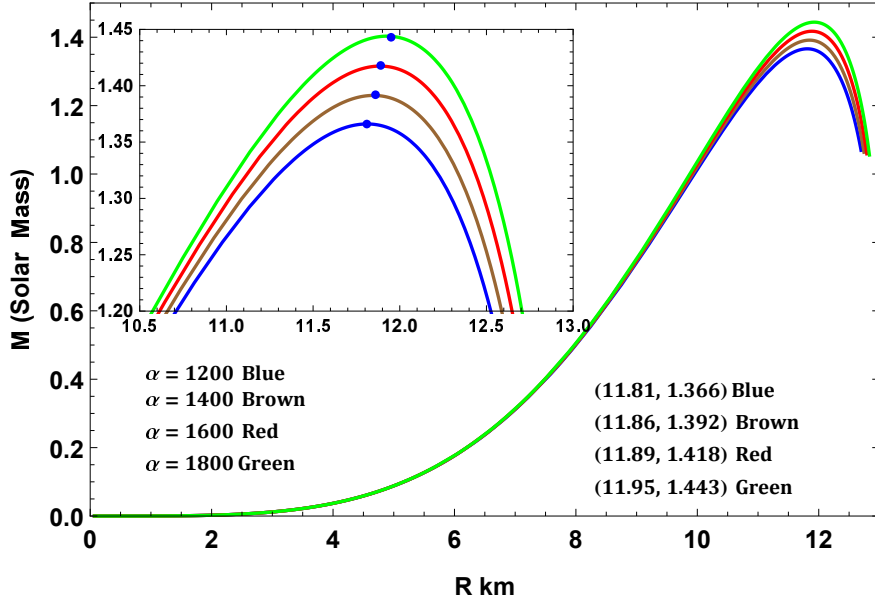


FIG. 12. $M - R$ graph assuming $M = 1.04M_{\odot}$, $R = 8.3km$ in EGB.

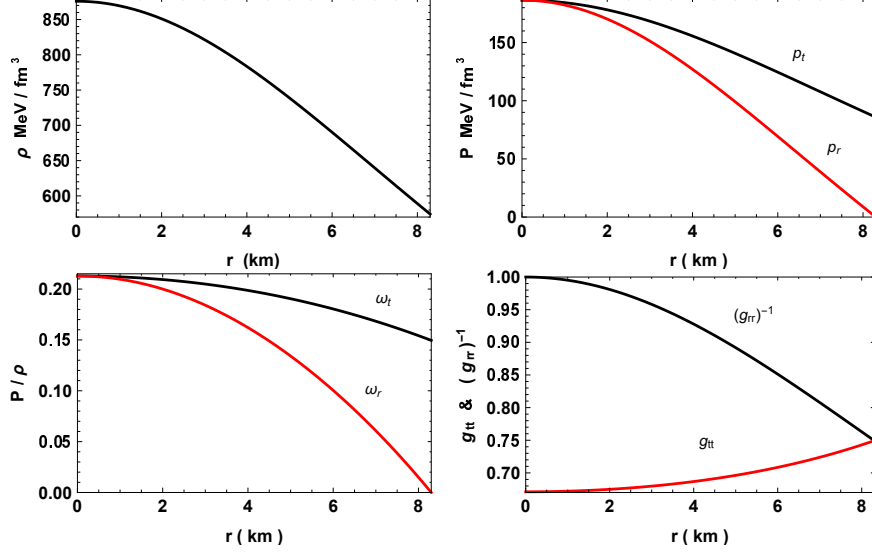


FIG. 13. Graphs of metric potentials, density, pressure and P/ρ for LMC X-4 with $M = 1.04M_\odot$, $R = 8.3\text{km}$ and $\gamma = 1/3$ in GR limit.

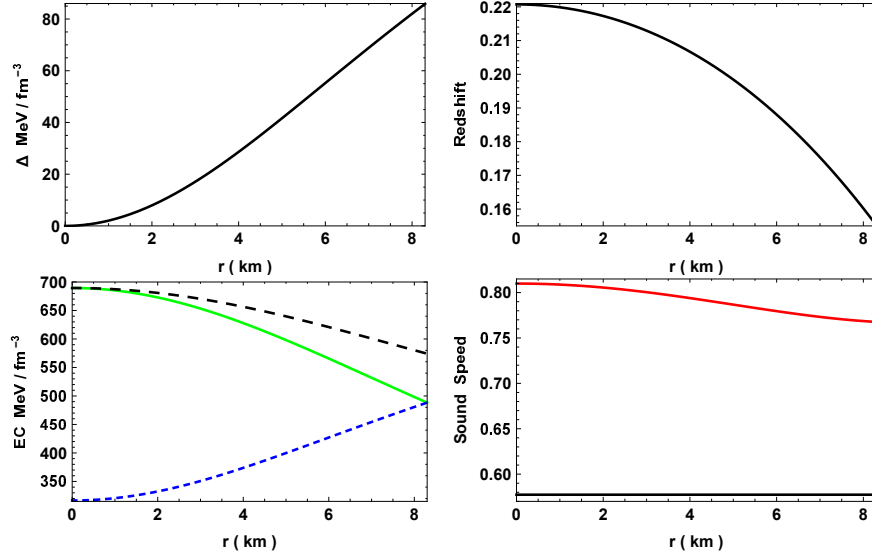


FIG. 14. Graphs of anisotropy, red-shift, energy conditions and sound speeds for LMC X-4 with $M = 1.04M_\odot$, $R = 8.3\text{km}$ and $\gamma = 1/3$ in GR limit.

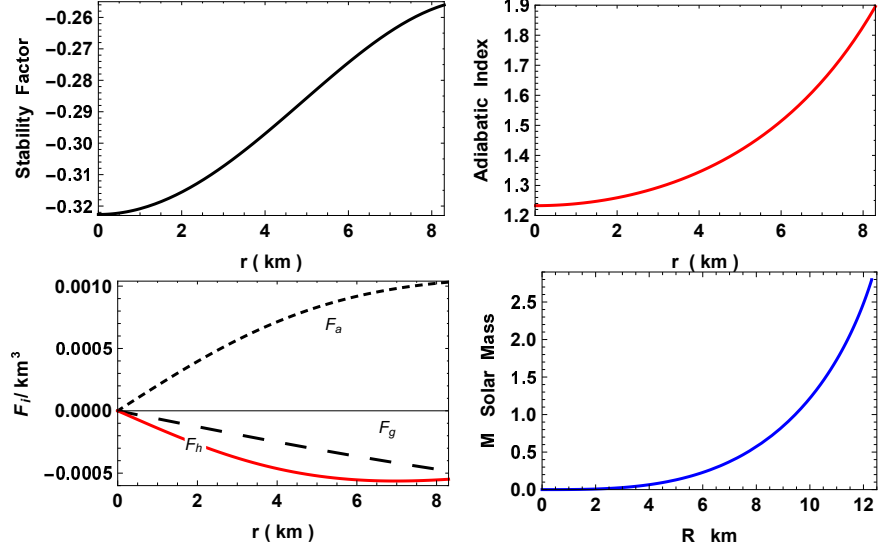


FIG. 15. Graphs of stability factor, adiabatic index, TOV-equation and $M - R$ curve with $M = 1.04M_\odot$, $R = 8.3\text{km}$ and $\gamma = 1/3$ in GR limit.

TABLE I. Parameter of few well-known compact star candidates

Object	$\frac{M}{M_{\odot}}$	R	γ	$c \times 10^{-3}$	α	χ	$\rho_c \times 10^{13}$	$\rho_b \times 10^{13}$	$p_c \times 10^{33}$
		km					g/cc	g/cc	$dyne/cm^2$
LMC X-4	1.04	8.3	0.33	0.161	1200	0.06885	7.15	6.99	8.68
SMC X-4	1.29	8.831	0.33	0.155	1250	0.07931	6.93	6.77	9.50
EXO 1785-248	1.3	8.849	0.33	0.154	1300	0.12468	6.89	6.77	1.06
4U 1820-30	1.58	9.1	0.33	0.163	1350	0.27091	7.52	7.32	1.78
PSR J1614-2230	1.97	9.69	0.33	0.158	1400	0.2788	7.32	7.13	1.93

VI. DISCUSSION

In this work we have generated the equations governing the dynamical evolution of astrophysical models in the Einstein–Gauss–Bonnet gravity paradigm with anisotropic stresses. After electing to use a strange star equation of state we employed the gravitational potential of Vaidya and Tikekar which was used to construct models of superdense stars in four dimensional gravity. The remaining gravitational potential was settled by solving differential equation emanating from the equation of state. It was then possible to calculate all the remaining dynamical variables and stability indicators. Graphical plots assisted us to investigate the behavior of the model with and without higher curvature effects. It was found that lower energy densities were realizable for increasing values of the coupling constant α . The pulsar LMC X–4 supplied mass and radius values to analyse other features of the star. It was also found that higher curvature terms resulted in a significant reduction in surface gravitational redshift values when compared to the 5 dimensional Einstein star. With regards to stability we concluded that the Gauss–Bonnet terms did not disturb the stability of the model in the Chandrasekhar adiabatic stability sense nor in the sense of the TOV equation components. Lower sound speeds were evident in the EGB models however neither model became acausal within the radial value. It was shown that the EGB model produced characteristics not out of sync with a range of known compact objects. This study demonstrates that the higher curvature Gauss–Bonnet terms should not be dismissed as corrections to the standard Einstein gravity theory.

-
- [1] Amendola L. , Charmousis C., Davis S. C. , 2007, JCAP 0710, **10** 004
 - [2] Abreu H., Hernández H., L.A. Núñez, 2007, Class. Quant. Grav., 24, 4631
 - [3] Bogdanos C., Charmousis C., Goutiaux B., Zegers R., 2009, JHEP , 0910, 37
 - [4] Boulware D. G., Deser S., 1985, Phys. Rev. Lett. , 55, 2656
 - [5] Bowers R. L., Liang E. P. T., 1974, Astrophys. J. , 188 657
 - [6] Buchdahl H. A., 1959, Phys. Rev., 116, 1027
 - [7] Buchdahl H. A., 1984, Class. Quant. Grav., 1, 301
 - [8] Caporaso G., Brecher K., 1979, Phys. Rev. D, 20, 1823
 - [9] Casadio R., Ovalle J., 2014, Gen. Relativ. Gravit., 46, 1669

- [10] Chan R., Herrera L., Santos N. O. , 1993, Mon. Not. R. Astron. Soc., 265, 533
- [11] Chandrasekhar S., 1964a, Astrophys. J., 140, 417
- [12] Chandrasekhar S., 1964b, Phys. Rev. Lett., 12, 114
- [13] Chilambwe B., Hansraj S., Maharaj S. D., 2015, Int. J. Mod. Phys. D, 24 1550051
- [14] Clifton T., Dunsby P., Goswami R., Nzioki A. M., 2013, Phys. Rev. D, 87, 063517
- [15] de Rham, C. *Living Rev. Relati* **17**, 7 (2014)
- [16] Dadhich N. K., Molina A., Khugaev A., 2010, Phys. Rev. D, 81, 104026
- [17] Davis S. C., 2003, Phys. Rev. D, 67, 024030
- [18] Duorah H. L., Ray R., 1987, Class. Quant. Grav., 4, 1691
- [19] Finch M. R., Skea J. E. F., 1989, Class. Quant. Grav., 6, 467
- [20] Ghosh S. G., Jhingan S., Deshkar D. W., 2014, J. Phys.: Conf. Series, 484, 012013
- [21] Govender M., Maharaj A., Lortan D., Day D., 2018, Astrophys. Space. Sci., 363, 165
- [22] Govender M., Mewalal N., Hansraj S., 2019, Eur. Phys. J. C, 79, 24
- [23] Govender M., Thirukkanesh S., 2015, Astrophys. Space Sci., 358, 8
- [24] Gross D., 1999, Nucl. Phys. Proc. Suppl., 74, 426
- [25] Hansraj S., Chilambwe B., Maharaj S. D., 2015, Eur. Phys. J. C , 27 277
- [26] Herrera L., 1992, Phys. Lett. A, 165, 206
- [27] Herrera L., Le Denmat G., Santos N.O. , 1989, Mon. Not. R. Astron. Soc., 237, 257
- [28] Herrera L., Le Denmat G., Santos N.O. , 2012, Gen. Relativ. Gravit., 44, 1143
- [29] Horndeski G. W., 1974, Int. J. Theor. Phys., 10, 363
- [30] Jhingan S., Ghosh S. G., 2010, Phys. Rev. D, 81, 024010
- [31] Kang Z., Zhan-Ying Y., De-Cheng Z., Rui-Hong Y., 2012, Chin. Phys. B, 21 020401
- [32] Karmarkar K.R., 1948, Proc. Ind. Acad. Sci. A, 27, 56
- [33] Kohler M., Chao K.L., 1965, Z. Naturforsch. Ser. A, 20, 1537
- [34] Koliogiannis P. S., Moustakidis C. C., 2019, Astrophys Space Sci, 364, 52
- [35] Mafa Takisa P., Maharaj S. D., 2013, Astrophys. Space. Sci., 343, 569
- [36] Maeda H., 2006, Phys. Rev. D, 73, 104004
- [37] Maharaj S. D., Chilambwe B., Hansraj S., 2015, Phys. Rev. D, 91, 084049
- [38] Maharaj S. D., Sunzu J., Ray S., 2014, Eur. Phys. J. Plus, 129, 3
- [39] Maurya S.K., Banerjee A., Hansraj S., 2018, Phys. Rev. D, 97, 044022

- [40] Maurya S. K., Banerjee A., Jasim M. K., Kumar J., Prasad A. K., Pradhan A., 2019, Phys. Rev D, 99 044029
- [41] Maurya S. K., Govender M., 2017, Eur. Phys. J. C, 77, 420
- [42] Maurya S. K., Ratanpal B. S., Govender M., 2017, Annals of Phys., 382, 36
- [43] Molina A., Dadhich N. K., Khugaev A., 2017, Gen. Rel. Grav., 49, 96
- [44] Myers R. C., Perry M. J., 1986, Ann. Phys., 172, 304
- [45] Myers R. C., Simons J. Z., 1988, Phys. Rev. D, 38, 2434
- [46] Perlmutter S. *et al.*, Supernova Cosmology Project collaboration, 1999, Astrophys. J., 517 565 [astro-ph/9812133]
- [47] Riess A. G. *et al.*, Supernova Search Team collaboration, 1998, Astron. J., 116, 1009 [astro-ph/9805201]
- [48] Tangherlini F. R., 1963, Il Nuovo Cimento, 27, 636
- [49] Torii T., Maeda H., 2005, Phys. Rev. D, 71, 124002
- [50] Vaidya P.C., Tikekar R., 1982, Journal of Astrophysics and Astronomy, 3, 325
- [51] Walecka J. D., 1975, Phys. Lett., 59, 109
- [52] Wheeler J. T., 1986, Nucl. Phys. B, 268, 737
- [53] Wright M., 2016, Gen. Re. Grav., 48, 93
- [54] Xian-Feng Z., Huan-Yu J., 2014, Revista Mexicana de Astronomia y Astrofisica, 50, 103

